Picosecond Microphotography as a Diagnostic Method for Laser Produced Plasmas

S. Ariga and R. Sigel

Max-Planck-Gesellschaft zur Förderung der Wissenschaften e. V.,
Projektgruppe für Laserforschung, Garching bei München

(Z. Naturforsch. **31 a**, 697–706 [1976]; received May 8, 1976)

A single picosecond pulse from a mode-locked dye laser was used for time resolved microphotography of the gasdynamic phenomena occurring in a lasertarget interaction experiment. A time resolution of 5 ps and a spatial resolution of better than 10 μm were experimentally obtained. Results are presented for the case of laser irradiation of a thin foil, shock wave propagation in a transparent target, expansion of the hot plasma and blast wave formation in a background gas.

1. Introduction

With the recent interest in laser fusion it has become clear that advanced diagnostic techniques will be needed to resolve the gasdynamic phenomena occurring on irradiation of solid targets. High-speed photography in the visible spectral range is of considerable interest in this context since it provides direct insight into the motion of the heated material during and after irradiation by a laser pulse. The microscopic size of laser-heated plasmas of $\sim 100\,\mu$m and their extremely short lifetime of $\sim 10^{-9}$ s call, however, for improved techniques with spatial resolution in the micron range and temporal resolution of the order of picoseconds. These requirements can be met with a pulse laser as light source in combination with high-resolution optics. Various arrangements have been used for this purpose and described in the literature [1–4].

In this paper we describe the application of a mode-locked dye laser for high-speed photography of the phenomena occurring on irradiation of plane solid targets with the Garching neodymium laser facility [5]. The advantage of using a dye laser for this purpose consists in its capability of generating very short pulses of 5 ps time duration, its relative simplicity and stability, the possibility of adjusting and testing the whole optical set-up independently of the main laser, and its convenient wavelength in the visible, where sensitive photographic material is available. Furthermore, the wavelength of the dye laser does not coincide with harmonics or subharmonics produced during nonlinear interaction of the main Nd laser beam with the plasma, which may outshine the phenomena to be observed, and in addition it may be tuned to match exactly the peak transmission of narrowband interference filters for maximum suppression of plasma self-luminosity. The paper deals mainly with the method itself and illustrates its advantages and limitations by means of a number of test results obtained in combination with a typical laser plasma experiment. To some extent we discuss also the physical nature of the phenomena observed since some of them have not been previously observed with such clarity. The application of the method to the investigation of laser heating of small pellets for filling magnetic traps has been described elsewhere [6].

2. Experimental Apparatus

A mode-locked dye laser made by Electro Photonics Co. of Northern Ireland was utilized as the light source for microphotography. This laser consists of a 5 mm diameter $\times$ 19.5 cm dye cell with Brewster windows pumped by a single flashlamp in elliptical configuration. Owing to stronger pumping of the cell side facing the flashlamp, the laser beam has an off-axial intensity distribution. This results in a reduction of the beam diameter to about 1/3 of the nominal cell cross-section. Ethanol solutions of Rhodamin 6G and DODCI (3,3 diethyloxadicarbocyanineiodide) were used for lasing and mode-locking, respectively. When mode-locked and tuned with an etalon, the laser generates a pulse train of $\sim 1.5\,\mu$s duration with about 300 pulses. The duration of each mode-locked pulse is a function of time, but normally less than 5 ps [7]. The maximum energy contained in a single pulse is less than 50 μJ. The wavelength was adjusted to 6050 Å ($\Delta\lambda \cong 10$ Å) and the time interval between successive pulses to 4.6 ns throughout this research.

A single pulse was selected from the mode-locked pulse train by an optical shutter consisting of two

Pockels cells and three Glan-Thomson prisms in series. A contrast ratio of 10 between the energy contained in a selected single pulse and the total radiation leaking through the closed shutter was measured. The low transmission of $\sim 10\%$ of the shutter resulted in the energy of a single pulse becoming less than 5 μJ.

The dye laser beam was directed by adjustable mirrors into the experimental chamber, where it illuminates the target at right angles to the main laser beam (see Figure 1). The target was imaged with $30\times$ magnification on Polaroid 3000 film. A Zeiss $F/2$ ($f=110$ mm) lens designed for diffraction limited resolution (~ 1.5 μm) at 6000 Å was used for this purpose. Owing to reflection losses from mirrors, windows and lens the pulse energy arriving at the film was only about 1 μJ.

The main laser for plasma production is the Garching neodymium laser facility [1, 5]. This generates single pulses of 5 ns duration at a wavelength of $\lambda = 1.06$ μm. The beam diameter at the last amplifier is 64 mm. It is focused on the target surface through an aspherical $F/1$ ($f=75$ mm) lens with a focal spot size of ~ 40 μm diameter. The laser was normally operated at a pulse energy of about 5 J throughout this investigation with a corresponding intensity in the focal spot of about 8×10^{13} W/cm^2. Previous investigations performed with this laser system have been reported elsewhere [1, 5].

Synchronisation between the dye laser and main laser was achieved in the following way (Fig. 1): First it was verified that the neodymium laser pulse and the mode-locked pulse train from the dye laser could be made coincident in time with a jitter less than 300 ns when the Q-switching Pockels cell in the Nd oscillator and the dye laser flashlamp were started by a common trigger pulse. Since the pulse train of the dye laser lasts for about 1.5 μs, a pulse from the dye laser would then always be available at the time when the main laser delivers its pulse on target. The final synchronisation was achieved with a fast photodiode which registered the Nd pulse immediately after leaving the optical shutter of the Nd laser. The signal of the photodiode gates by means of Krytron trigger circuit the optical shutter of the dye laser. The U-shaped set-up of the Nd laser with 100 ns travelling time of the Nd pulse from shutter to target, installation of the dye laser close to the Nd oscillator and fine adjustment by a cable of variable length between photodiode and dye laser shutter ensured that despite a 20 ns internal delay in the Krytron trigger a dye laser pulse could arrive at the target slightly before, during or at any time after the Nd pulse.

Whereas in this way the dye laser shutter and the Nd pulse could be synchronized with a jitter of less than 1 ns, this does not mean that a selected dye laser pulse reaches the target at an exactly predetermined time. This is because the dye laser is passively mode-locked and hence, when gating the dye laser shutter at a given time, the pulses of the mode-locked pulse train will have a jitter relative to the gate equal to the distance between successive pulses in the train. As was mentioned above, the pulse distance was 4.6 ns and the gate duration was correspondingly set to the same duration in order to ensure selection of only a single pulse with a probability near one. Since it is important to know exactly the time when a photograph has been taken, the arrival of both the Nd dye laser pulse at the target were registered by a common photodiode. The oscillograms thus obtained with a Tektronix 519 oscilliscope allowed correlation of the photographed phenomena with the Nd pulse (Figure 2).

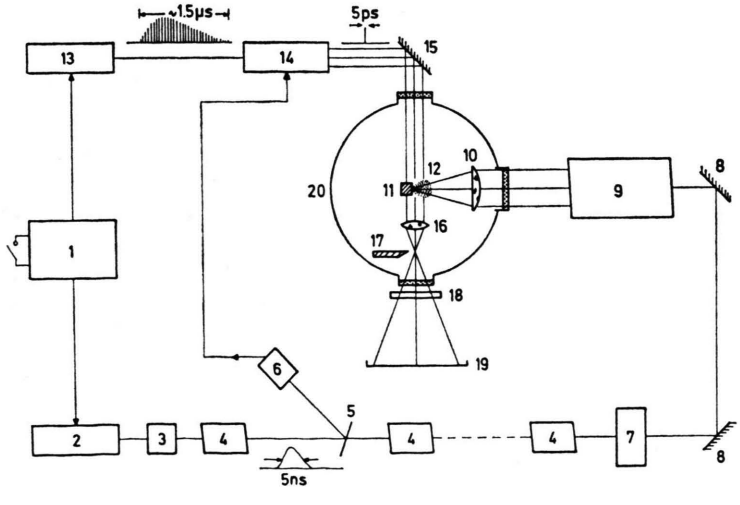

Fig. 1. Schematic diagram of the experimental set-up;
1 — main controller, 2 — Nd glass laser oscillator, 3 — pulse-shaping system, 4 — amplifiers, 5 — beam splitter, 6 — photodiode, 7 — Faraday rotator, 8 — surface mirrors for 1.06 μm, 9 — last amplifier, 10 — aspherical lens, 11 — target, 12 — plasma, 13 — dye laser oscillator, 14 — pulse selecting system, 15 — mirror, 16 — objective lens, 17 — schlieren blade, 18 — interference filter, 19 — Polaroid film, 20 — chamber.

The time evolution of the phenomena under investigation could then be obtained from a series of photographs taken at random, but well known times which later were ordered into proper succession.

When taking photographs with the system it was noticed that self-luminosity of the plasma overexposed the film. Insertion of a 20 Å narrow band interference filter into the imaging system reduced self-luminosity from a copper target to $\sim 2\,\mu$J, this still being of the same order as the energy of the dye laser pulse. It was thus necessary to diminish the lens aperture to $F/8$ in order to reduce film exposure by the isotropically emitted plasma light to a tolerable level. The resolution of the lens was therefore limited by diffraction to $\sim 10\,\mu$m.

3. Experimental Results

The method described above was applied to study the phenomena occurring during the interaction of powerful laser radiation with a plane solid target. For convenient understanding of the following results the interaction may by described briefly as follows[1]: The focussed laser radiation rapidly ionizes and heats surface material and creates a dense and hot plasma cloud. Since the plasma is not confined towards the vacuum side it will immediately begin to expand. If, as in the present experiment, the laser pulse duration is larger than $\tau \gtrsim R/C_s$ (τ = laser pulse duration, R = radius of the irradiated area, C_s = sound velocity in the plasma) a quasistationary plasma outflow from the irradiated area will be established which lasts for the laser pulse duration. Heating occurs in the dense part of the plasma in the vicinity of the so-called critical electron density n_{ec}, defined by

$$\omega_L = \omega_{pe} = (e^2 n_{ec}/\varepsilon_0 m_e)^{1/2}$$

(ω_L = laser frequency, ω_{pe} = electron plasma frequency). In the case of heating with a Nd laser pulse, the critical density has the value of $n_{ec} = 10^{21}\,\mathrm{cm}^{-3}$. From previous measurement the electron temperature is typically $kT_e \cong 300$ eV under the present experimental conditions.

The pressure exerted by the hot and dense plasma on the neighbouring solid material will cause a shock wave in the target. Pressure in the megabar range and a compression of the material to several times solid state density are readily achieved under the present experimental conditions[8]. Since the driving plasma "piston" is of small lateral extent the shock wave will rapidly assume a hemispherical shape and, after termination of the laser pulse, propagate as a blast wave of decreasing strength into the interior of the target.

In the following we present several examples which demonstrate the potential of high-speed photography in laser produced plasma experiments.

A) Acceleration of a Thin Foil

The method was first applied to irradiation of copper foils with a thickness of 50 μm and 100 μm. Results are shown in Figure 3. Irradiation of the foil by the main laser is from the right. The foil is slightly bent and thus only the rear side is observed, where breakthrough of the shock wave through the foil occurs. The front side of the foil with the plasma is obscured in this case and hence the problem of plasma self-luminosity avoided.

Under the impulsive load of the laser produced plasma, foil material is accelerated towards the rear, breaks up after about 100 ns and finally disintegrates into a (possibly hollow) jet of fine particles. After about 400 – 900 ns (the last two pictures) this process is nearly terminated and the hole left in the foil has reached its final diameter of $\sim 500\,\mu$m. The velocity of the particles on the axis is $V_p = 2 \times 10^5\,\mathrm{cm\,s}^{-1}$ and constant in time. It should be noted that all the pictures in Fig. 3 were taken long after termination of the laser pulse.

In the focal plane the spatial resolution for the given magnification, film grain etc. is about 10 μm. Since the depth of the field of view is limited with a high aperture lens as applied here (the lens was used with full aperture in this case) no attempts were made to make use of the full resolution of the optical system. As may be noted, many of the particles are already out of focus and show the fringe structure characteristic of laser illumination. As expected, for the short pulse (~ 5 ps) of the dye laser the motion of the material is absolutely frozen.

The accelerated foil material acquired its momentum by the driving "plasma piston" which exerted a pressure p for a time τ on the foil material (the loss of foil material by plasma expansion can be neglected[1]). For our relatively long main laser pulse τ may be assumed equal to the laser pulse duration and hence we can estimate the accelerating pressure by

$$p \cong \varrho\, D\, V_p/\tau$$

where $\varrho = 9\,\mathrm{g\,cm}^{-3}$ and $D = 50\,\mu$ are the density

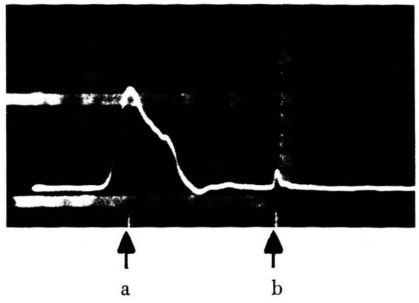

Fig. 2. Oscillogramm of neodymium (a) and dye (b) laser pulse. 10 ns/div.

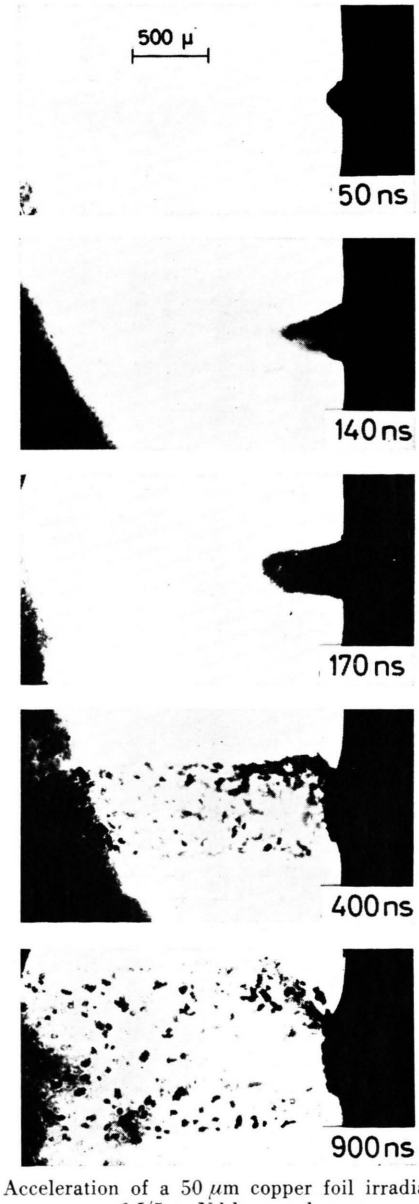

Fig. 3. Acceleration of a 50 μm copper foil irradiated with a 6 J/5 ns Nd laser pulse.

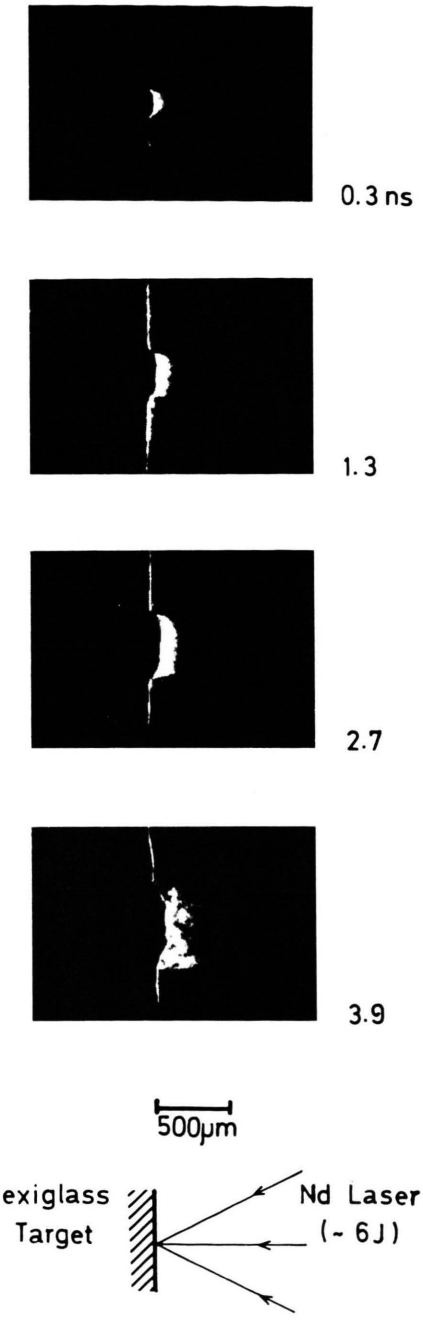

Fig. 4. Dark-field schlieren photographs of a laser-produced plasma at the surface of a plexiglass target.

and thickness of the copper foil respectively. With $V_p = 2.5 \times 10^5$ cm s^{-1} and $\tau = 5$ ns we find $p = 1.8$ Mbar. This estimate is in quite reasonable agreement with shock wave measurements during the laser pulse described in [8].

B) Plasma Formation on the Target Surface

In another experiment a plexiglass (polymethyl methacrylate $(C_5O_2H_8)_n$) target was irradiated with a 6 J/5 ns Nd laser pulse. The target consisted of a vertical rod with a diameter of 2 mm. This type of target ensures the possibility of tangential observation of surface phenomena but may still be considered as plane over the irradiated area (note that in cases where we are interested in the phenomena occurring in the interior a target with a concave surface was chosen; see Figure 6). A vertical schlieren blade was introduced in the optical path at the focus of the dye laser beam between the lens and film. A series of dark-field schlieren pictures is shown in Figure 4. Emphasis is now on the plasma which is formed at the front surface of the target. With the dark-field schlieren technique plasma regions with a density gradient appear bright in the photograph. The series of photographs in Fig. 4 was taken during the main laser pulse.

The dye laser system allowed the first picture to be taken at a time $t = 0.3$ ns after the pulse begins to rise on the oscilloscope (Figure 2). At the time where the total impinged energy is estimated to be less than 20 mJ a plasma cloud has already formed at the target surface with a lateral extent equal to the focal spot diameter. During the rise of the pulse to its maximum intensity the lateral extent of the plasma increases rapidly with a velocity parallel to the target surface of more than 2×10^7 cm s^{-1}. This phenomenon may be caused by lateral heat conduction, which transports energy from the centre of the focal spot to the plasma produced in the wings of the focal spot intensity distribution and hence causes ablation over a much larger area than actually irradiated with high intensity.

The series of photographs in Fig. 4 again demonstrates the high spatial and temporal resolution of the method. But also a limitation of the present equipment is apparent from Fig. 4, especially from the last photograph ($t = 3.9$ ns). This concerns the intensity fluctuations seen in the region of the expanding plasma, which might be due either to random density gradients in the plasma or to the nonuniform intensity distribution of the multimode dye laser beam.

From a larger number of photographs as in Fig. 4 taken with varying schlieren blade positions the time evolution of the plasma density profile along the optical axis of the main laser beam was constructed (Figure 5). Instead of the blade position, the deflection angle α^0 (in degrees) corresponding to the bright/dark transition at the vacuum boundary of the plasma is given. α^0 was correlated with the local plasma density by assuming a spherically expanding plasma with a radial decrease in density of the form r^{-2} (see [9]).

As can be seen in Fig. 5, the density profile approaches a stationary state, the dense part of the plasma more rapidly than the low density part. The highest density measured is 1.1×10^{20} cm^{-3}, which is one order of magnitude lower than the critical density. This upper limit is set by the fact that light rays traversing the denser part of the plasma are

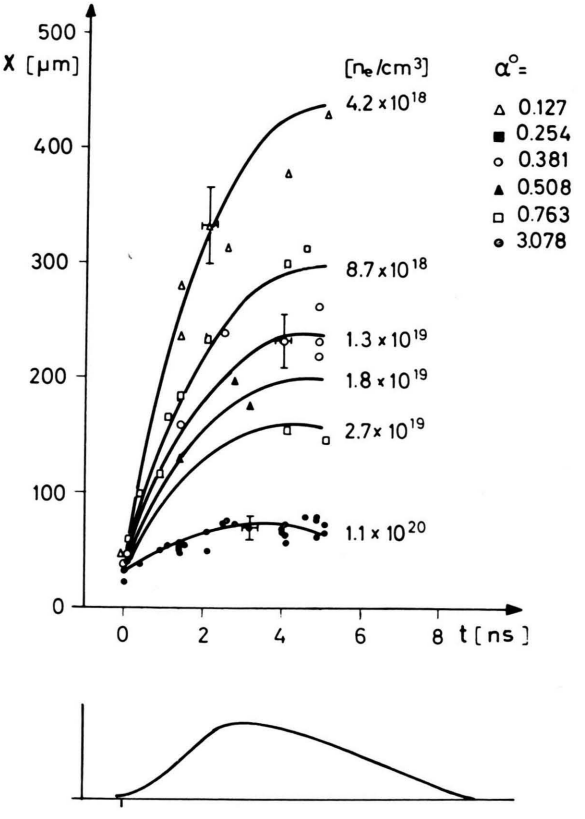

Fig. 5. Electron density distribution in front of the plexiglass target as a function of time. The pulse shape of the main laser pulse is indicated at the bottom.

deflected out of the aperture of the objective. An extrapolation of the density profile towards the target suggests that the critical density layer is located just in front of the target surface in agreement with X-ray pinhole measurements [5].

C) The Laser-driven Shock Wave

As was mentioned above, the high pressure exerted by the plasma leads to the formation of a shock wave which propagates into the interior of the target. It was observed first in [8] using an ultra-fast streak camera. Here we demonstrate that the shock wave can be investigated with much superior resolution using the present method.

Figure 6 shows the propagation of the shock wave into a solid deuterium target at various times during and after the laser pulse. Owing to the special shape of the target the area to the right of the solid-vacuum interface appears dark. As was evaluated in [8], initially a pressure of ~ 2 Mbar and a compression of the solid material of $4-5$ is achieved. Under such conditions the material behind the shock front is found to be opaque to the dye

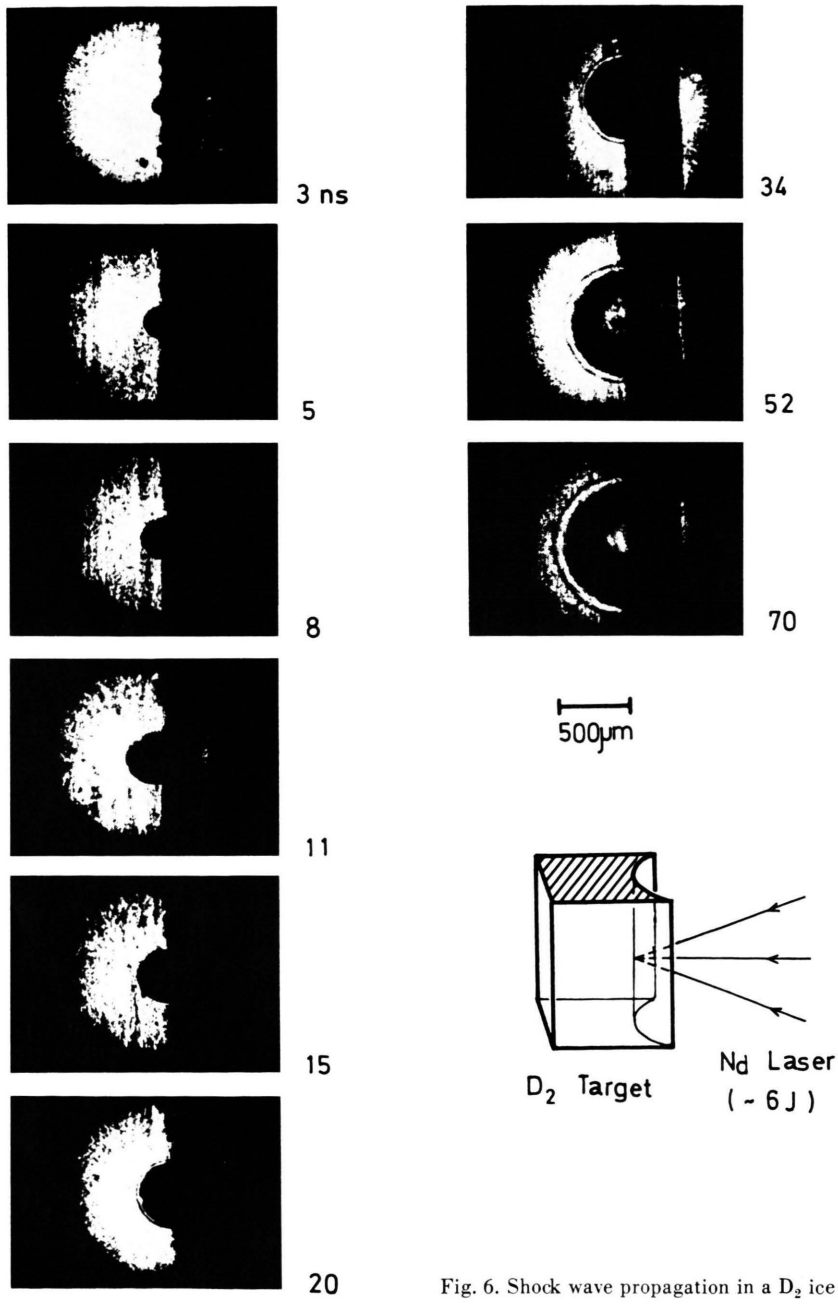

Fig. 6. Shock wave propagation in a D_2 ice target.

laser light, probably as a result of ionization due to the strong shock compression. After termination of the laser pulse the velocity of the shock wave, and hence the pressure behind the shock front, drop rapidly. Thus, after about 11 ns, the material behind the front remains transparent under shock compression and the shock front becomes visible. Whereas the shock front propagates still further into the target, the material encompassed initially by the shock front already begins to expand towards the vacuum side. At about 50 ns the conditions are obviously such that the dye laser light can penetrate again through the region where the shock wave had its origin.

Figure 7 shows the phenomenon at a still later time (200 ns) in a plexiglass target. The shock wave is now remote from the point of impact of the laser beam, near which an opaque zone is left extending into the interior of the target. The dimensions of this zone corresponds approximately to the dimensions of the crater which is left in the target. But still dense material slowly expands towards the vacuum, causing a crown-like shadow on the picture. It may be noted that the phenomenon at such a late time is similar to a hypervelocity impact onto the target [10, 11].

For further details concerning the laser-driven shock wave we refer to [8]. The examples presented here may demonstrate that the present method also enables us to investigate this phenomenon with high spatial and temporal resolution.

D) Blast Wave Formation in a Background Gas

If the laser irradiated target is surrounded by a low-pressure gas the expanding plasma will produce a strong blast wave in the gas. Observation of the blast wave is of interest because its radius versus time history may be used to determine the energy absorbed in the target [2, 12].

Experiments were carried out with a plane copper target surrounded by helium gas with a pressure in the range 20 – 300 torr. The darkfield schlieren technique was used with the pulse selection system of the dye laser set so that it transmitted several pulses in order to obtain several pictures of the shock front [13] at precisely known time intervals of 4.6 ns. Figures 8 a, b shows examples for the early (a) and later stages (b) of blast wave propagation in 50 torr helium gas. Though the velocity of the blast wave is initially as high as 2×10^7 cm s^{-1}, it will move only 1 μm during the 5 ps duration of a dye laser pulse and hence the blast wave is still depicted without any loss of resolution despite its rapid motion.

The blast wave in Fig. 8 a, b has a fairly regular shape though local disturbances may be noted. Sometimes we observe, however, that the blast wave is heavily disturbed in some regions. An example is presented in Figure 9. Here the blast wave is hardly visible in a cone around the optical axis. Closer inspection shows that a tongue-like, rather vague blast wave propagates ahead of the main front. It was supposed that this behaviour occurs owing to preheating of the gas by gas breakdown due to the action of the main laser beam. To check this assumption, experiments were performed at higher gas pressure (300 torr) with the target present (Fig. 10 a) or removed sideways out of the main laser beam path (Figure 10 b). In the presence of the target the blast wave becomes very irregular at such high pressure (Figure 10 a). With the target removed, gas breakdown occurs. The special shape of the blast wave produced by gas breakdown (Fig. 10 b) may be recognized again in the case where a target is present (Figure 10 a). Thus, we conclude that gas breakdown and preheating of the gas is at least partly responsible for the observed irregularities in blast wave propagation. The fairly irregular shape of the blast wave initiated by gas breakdown (Fig. 10 b) may be connected with the fact that in this series of experiments the intensity of the main laser beam was anomalously high in cones much narrower than the aperture of the focusing lens owing to the presence of hot spots in the main laser beam.

From a series of photographs taken at a gas pressure of 50 torr the radius versus time history of the blast wave was plotted in Fig. 11 for various angles to the optical axis. It is noted that during an initial stage (up to 20 ns) the radius of the blast wave increases about linearly with time ($\Theta = 0^\circ$). In this range the mass of the gas collected by the blast wave is small or just becomes comparable to the mass of the gas collected by the blast wave and hence the gas is simply pushed ahead with the velocity of the expanding plasma. At a later stage (~ 20 ns) where plasma production is long terminated and the mass of the gas has become greater than the plasma mass, the experimental curves

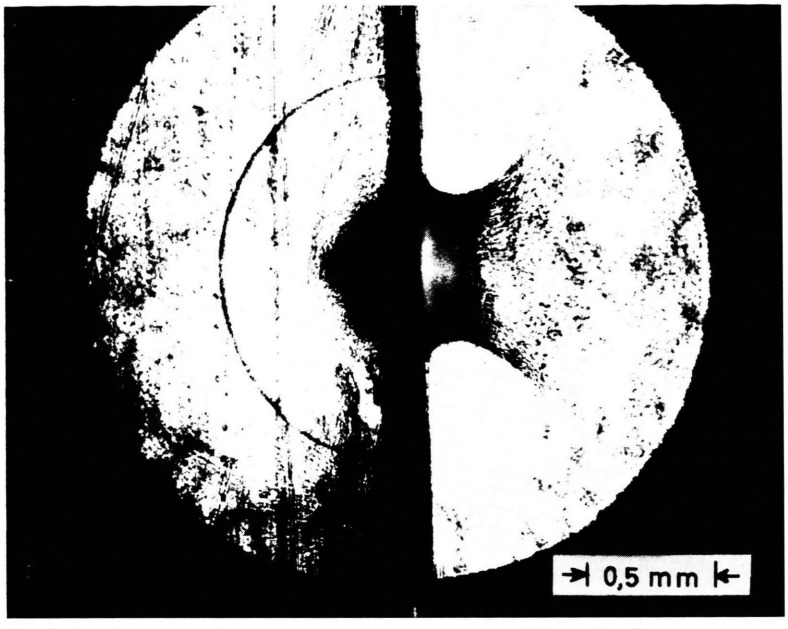

Fig. 7. Shock wave and crater in a plexiglass target 200 ns after laser impact.

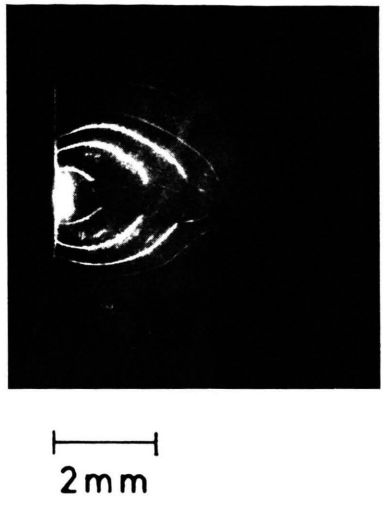

Fig. 9. Disturbed blast wave (50 torr helium). First dye laser pulse at $t =$ 5 ns.

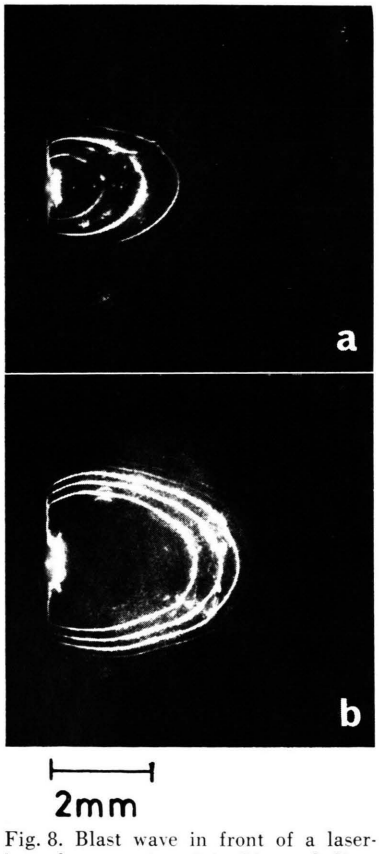

Fig. 8. Blast wave in front of a laser-heated copper target in 50 torr helium background gas. a) First dye laser pulse at $t = 6.5$ ns; b) first dye laser pulse at $t = 16.8$ ns.

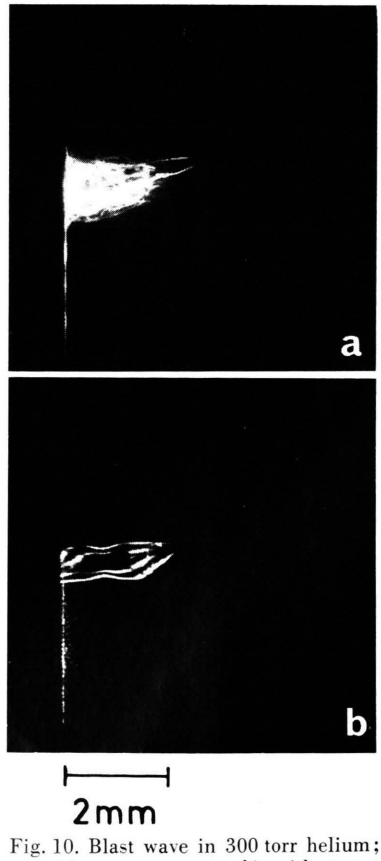

Fig. 10. Blast wave in 300 torr helium; a) with copper target, b) with target out of beam.

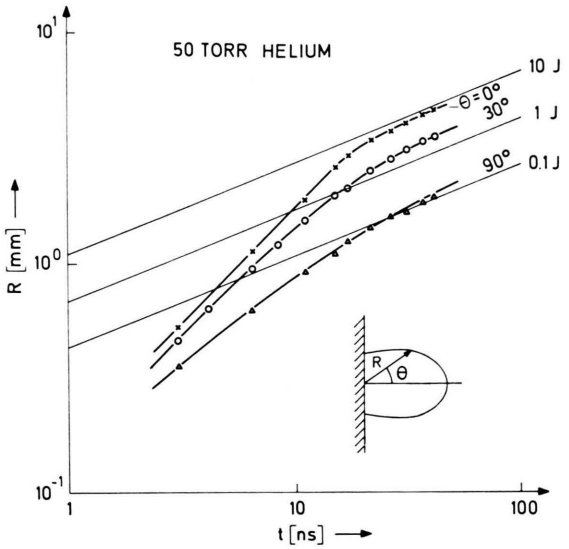

Fig. 11. Radius of blast wave versus time for various angles. Straight lines are calculated with the blast wave formula Eq. (1) for various energies.

asymptotically approach the dependence predicted by the blast wave formula [10]

$$R(t) = \xi (E/\varrho)^{1/5} t^{2/5}, \qquad (1)$$

where $\xi = 1.12$ for a fully ionized gas with $\gamma = 5/3$, E the energy contained in the blast wave and ϱ the density of the undisturbed gas.

The $R(t)$ dependence of Eq. (1) was plotted for several values of E in Figure 11. It is apparent that the experimental curves approach widely different values of E, depending on the angle Θ. This is a consequence of the fact that the test experiments with plane targets described here do not correspond to the spherical symmetry underlying Equation (1). An attempt was made to estimate the blast wave energy for the geometry of the experiment by weighting the contributions corresponding to different angles Θ. For the model described in Appendix A one recovers about 17% of the incident laser energy. Typically 20% of the incident laser radiation are known to be lost by back reflection through the focussing lens. It is tempting to speculate that, besides radiation and ionisation losses from the plasma and compressed gas [2], scattering losses of laser radiation may account for the missing part of the energy. Any conclusive interpretation would, however, first need an accurate two-dimensional evaluation of blast wave propagation for the geometry of the experiment. This is beyond the scope of this paper, where we are mainly interested in the method itself rather than in quantitative aspects of plane target experiments.

4. Summary

In this paper we have demonstrated that a mode-locked dye laser system is a suitable light source for high-speed photography with high spatial and temporal resulution. The pulse duration of ~ 5 ps readily available from such a laser is short enough to "freeze" even the most rapid motions of matter occurring in laser-target experiments. The spatial resolution of 10 μm achieved could even be increased further to the diffraction limit of the lens (~ 1.5 μm) if this is desirable with respect to the limited depth of the field of view. The examples presented demonstrate that indeed a large number of interesting phenomena can be investigated in the case of laser-produced plasmas by high-speed photography in the visible range.

It became also apparent during the course of the investigation that improvements of the system in several respects would be desirable. If means for a more accurate synchronisation could be found this would ease investigation of single, irreproducible events. Also to increase the brightness of the system would be most desirable. This concerns the problems of self-luminosity and speckles mentioned above and possible applications to interferometry. Measures to increase the brightness could consist in better mode control of the oscillator, further amplification of the pulse and reduction of losses in the optical system. With corresponding improvements the technique described here could become an even more valuable tool for high speed photography of ultrafast phenomena.

Acknowledgements

The authors express their thanks to Dr. S. Witkowski, Dr. P. Mulser, and Dr. K. Eidmann for their fruitful suggestions throughout this work. Thanks are also to Dr. H. C. Pant and Dr. C. G. E. van Kessel for their helpful collaboration. The assistance of P. Sachsenmaier, E. Wanka, and H. Brändlein is gratefully acknowledged. This work was performed under the terms of the agreement on association between Max-Planck-Institut für Plasmaphysik and Euratom.

Appendix A

The shape of the blast wave is modelled by

$$R(\Theta) = R_0 \cos \Theta ,$$

i. e. as a spherical wave with its centre at $R = R_0/2$. Since in each direction Θ the distance from the origin approaches the typical blast wave behaviour $R \sim t^{2/5}$, the experimental blast wave is assumed to be made up of a large number of blast waves with their centre at the origin (see Figure A1). The energy dE contained in a surface element dF obtained by rotation of δ around the R-axis is then given by

$$dE = E(R)\, dF/4\pi R^2 = E(R)\, 2\pi R^2 \sin\Theta\, d\Theta / 4\pi R^2 = \tfrac{1}{2} E(R) \sin\Theta\, d\Theta ,$$

where $E(R)$ is given by Equation (1).

Integration yields for the blast wave energy E_B

$$E_B = \int_{\Theta=0}^{\pi/2} dE = \tfrac{1}{2} E_0 \int_{\Theta=0}^{\pi/2} \cos^5\Theta \sin\Theta\, d\Theta = \tfrac{1}{12} E_0 ,$$

where E_0 is given by $E(R_0)$.

Thus, E_B is only 1/12 of the energy of a blast wave with radius R_0 centered at the origin, i. e. 1/12 of the energy approached asymptotically by the curve $\Theta = 0^\circ$ in Figure 11. Results obtained in this manner for three shots with gas pressures in the range 21 – 100 torr are given in Table A1.

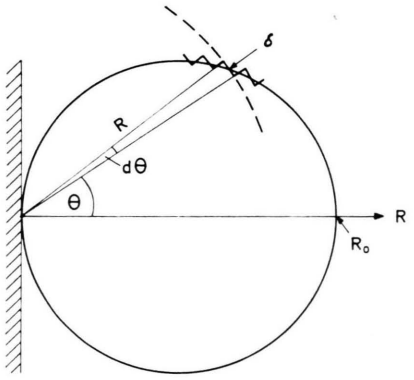

Fig. A1. The model for blast wave evaluation.

Table A1. Blast wave data.

Helium Gas Pressure	Nd Laser Energy	Estimated Blast Wave Energy E_B	% of Laser Energy
21 torr	6.0 J	0.97 J	16
50 torr	5.0 J	0.83 J	17
100 torr	3.5 J	0.59 J	17

[1] For a review of laser-produced plasmas see P. Mulser, R. Sigel, and S. Witkowski, Physics Reports (Section C of Physics Letters) **6**, 187 [1973].

[2] N. G. Basov, E. G. Gamaly, O. N. Krokhin, Yu. A. Mikhailov, G. V. Sklizkov, and S. I. Fedotov, Laser Interaction and Related Plasma Phenomena, H. Schwarz and H. Hora eds. (Plenum Press 1974), Vol. 3B, p. 553.

[3] Laser Program Annual Report 1974, Lawrence Livermore Laboratory, Rep. UCRL-50021-74 [March 75].

[4] D. Kohler, D. Giovanielli, R. P. Godwin, G. H. McCall, and M. M. Mueller, Bull. APS II, **19**, 854 [1974].

[5] K. Eidmann, C. van Kessel, M. H. Key, P. Mulser, R. Sigel, Plasma Physics and Controlled Nuclear Fusion Research [1974], International Atomic Energy Agency, Vienna 1975, Vol. II, p. 357.

[6] S. Ariga, K. Büchl, and T. Häring, Max-Planck-Institut für Plasmaphysik, Laboratory Report IPP 4/129 [January 1975].

[7] E. G. Arthurs, D. J. Bradley, and A. G. Roddie, Appl. Phys. Lett. **23**, 88 [1973].

[8] C. G. M. van Kessel and R. Sigel, Phys. Rev. Lett. **33**, 1020 [1974]; C. G. M. van Kessel, Z. Naturforsch. **30 A**, 1581 [1975].

[9] R. Kinslow, ed., High Velocity Impact Phenomena, Academic Press, New York 1970, Chap. IV.

[10] Ya. B. Zeldovich and Yu. P. Raizer, Physics of Shock Waves and High Temperature Hydrodynamic Phenomena, Academic Press, New York 1965.

[11] T. A. Leonard and F. J. Mayer, KMS Fusion Inc., Laboratory Report KMSF-U 309.

[12] A. J. Alcock, C. de Michelis, K. Hamel, and B. A. Tozer, J. QEEE, **QE-4**, 593 [1968].

[13] V. L. Ginzburg, The Propagation of Electromagnetic Waves in Plasmas, Pergamon Press, London 1964, p. 409.